Math. Model. Nat. Phenom. 18 (2023) 19
https://doi.org/10.1051/mmnp/2023021

Mathematical Modelling of Natural Phenomena
www.mmnp-journal.org

HEAT AND MASS DIFFUSION TO WILLIAMSON FLUID STREAMING THROUGH A TUBE WITH MULTIPLE STENOSES WHILE SUBJECTED TO PERIODIC BODY ACCELERATION

Muhammad Fahim*, Muhammad Sajid, Nasir Ali and Muhammad Noveel Sadiq

Abstract. This article examines a mathematical framework that describes the versatile behavior of heat and mass exchange in blood flowing through a narrowed vessel having multiple stenoses. The geometry of a channel having multiple stenoses with an asymmetrical axial axis and a symmetrical radial axis can be visualized by applying a suitable mathematical expression. The geometry of the chosen model considers the height and shape of stenoses. The modification in shape parameter is used to capture variations in the shape of the stenoses in the artery. The blood is supposed to be isochoric (incompressible), while its rheological behavior is characterized by Williamson's fluid model. The transfer of momentum is analyzed using the equation of motion in cooperation with the continuity equation. In addition, the equations of heat conduction and diffusion are utilized, respectively, to illustrate the distributions of heat and mass. Simplified forms of momentum, mass, and heat transport equations are achieved by incorporating dimensionless quantities and moderate stenosis conditions. A well-known explicit finite difference approach is utilized to solve the emergent non-linear system of governing equations numerically. The influence of different evolving parameters on the flow field along with mass and heat distributions is illustrated through various plots.

Mathematics Subject Classification. XXX.

Received October 17, 2022. Accepted June 28, 2023.

1. Introduction

The cardiovascular system plays a vital role in the human body by transporting oxygen and nutrients, removing wastes, and regulating body temperature. Unfortunately, many cardiovascular diseases can be fatal, and in 2018 alone, the World Health Organization reported more than 17.8 million deaths due to various vascular illnesses. These diseases often result from high levels of fat and abnormal growth and deposition in blood vessels, leading to stenosis or artery narrowing. One of the most common causes of stenosis is the accumulation of low-density lipoprotein in the artery wall, particularly in areas of the vascular system where blood flow patterns vary, such as bends, bifurcations, and other key areas.

Researchers have extensively studied blood flow behavior in stenosed arteries, particularly in moderate stenosis. For example, Young [42] was among the first to analyze blood flow patterns in stenosed arteries. In addition,

Keywords and phrases: Blood flow, multiple stenosis, heat and mass exchange, body acceleration, finite difference approach.

Department of Mathematics and Statistics, International Islamic University, Islamabad, Pakistan.

* Corresponding author: fahim.muh1@gmail.com

Forrester and Young [13] examined the impact of tapering angles on isochoric fluid flow in an axisymmetric channel. Chow and Soda [10] discussed boundary irregularities' effects on blood flow. Azuma and Fukushima [6] conducted an empirical study to identify blood flow patterns in various arterial stenosis geometries. Some other studies have examined the steady-state behavior of blood flow in moderate arterial stenosis [22], as well as the influences of periodic body acceleration on the pulsating flow of blood in circular tubes [43]. Despite these diverse investigations, blood rheology in the literature mentioned above is limited to Newtonian fluids.

However, the available literature on hemodynamic investigations shows that blood cannot always be characterized as a Newtonian fluid, and that blood expresses significant non-Newtonian features such as viscoelastic, yield stress, shear-thinning, and thixotropic under specific conditions, such as in small arteries with moderate shear rates, infected arteries, and pulsating flow scenarios. Many numerical and theoretical investigations of non-Newtonian blood flow have been reported. For instance, the power-law model exhibits appreciable non-Newtonian behaviors at reasonable shear rates, as reported by Perktold *et al.* [30]. However, this model is insufficient to reflect behavior at extreme shear rates. This gap may be bridged by choosing appropriate models such as Sisko, Cross, Eyring Powell, and Carreau, *etc.* Many other studies have been conducted to analyze the influence of external factors, such as body acceleration, curvature, and magnetic field, on blood flow through stenotic tubes. For example, Mandal and Kumar [21] presented a bi-dimensional mathematical model investigating the influence of externally induced periodic body acceleration on the blood flow of generalized power law fluid through an elastically stenosed artery. Ismail *et al.* [14] analyzed the key factors of non-Newtonian power-law blood, showing that blood behaves non-Newtonian when the arterial radius is less than one millimeter. Nagarani and Sarojamma [27] examined the influence of body acceleration on the pulsating flow of Casson fluid via a moderately stenosed channel. Numerous studies [32]–[28] have utilized analytical and numerical methods to model the behavior of non-Newtonian blood flow through stenotic tubes, considering a range of parameters and external factors. These studies can help to enhance our understanding of cardiovascular diseases and pave the way for improved diagnosis and treatment.

The studies mentioned above considered moderate stenosis with a single geometric shape, typically a cosine curve, and a small depth-to-vascular radius ratio. However, in reality, patients with multiple stenoses in the same arterial system are quite common. Several studies, including those cited in references [17]–[12], have investigated the impacts of multiple stenoses on blood flow. These studies suggest that the overall impact of non-critical stenoses can be comparable to the sum of their individual effects, which can be life-threatening or cause physical problems related to arterial fatigue. Studies [20]–[31] also examined the impact of multiple stenoses on blood flow, however, they did not consider mass transport.

The rheological behavior of non-Newtonian fluids cannot be fully explained by classical Navier-Stokes equations alone. As a result, numerous models have been formulated to depict the properties of such fluids. One of the earliest models was introduced by Williamson [41] in 1929. This model provides a clear and concise simulation of the viscoelastic shear-thinning features of non-Newtonian fluids. According to this model, the effective viscosity of the fluid must decrease infinitely as the shear rate increases. It should have infinite viscosity at rest and zero (null) viscosity as the shear rate approaches infinity. In recent years, researchers have focused on the Williamson model to understand the nature of non-Newtonian fluids. Some recent studies have highlighted the mass and heat exchange in Williamson nanofluid [18], the peristaltic motion of Williamson fluid via an unsymmetric conduit with porous walls [37], the peristaltic transport of the chymus characterized by the Williamson model in a small intestine [26], and Brownian diffusion and thermophoresis in a Williamson fluid subjected to magnetohydrodynamic blood flow through a radiative wedge [35]. For further knowledge of the Williamson model, one may refer to the suggested references [1]–[33].

By conducting experimental and theoretical studies on the impacts of heat/mass transport on hemodynamics, researchers have gained a better understanding of the complex mechanisms underlying vascular disorders, such as arteriosclerosis. Caro *et al.* [9] hypothesized that arteriosclerosis might occur due to the mass exchange process between arterial walls and blood. Back *et al.* [7] quantitatively investigated the impacts of mass transfer on unsteady two-dimensional blood flow through the coronary artery. Chakravarty and Sen [8] provided a mathematical model to represent the temporal responses of mass and heat exchange in blood flowing through bifurcated stenotic channels. Victor and Shah [38], [39] investigated the implications of heat diffusion for a fully

developed stream at the tube inlet section. They suggested suitable Prandtl number values associated with heat exchange in the bloodstream. Abbey and Ogulu [29] analyzed the modeling of heat convection in blood passing through a stenotic vessel, while Zaman *et al.* [45] evaluated the impacts of mass and heat transport on the bloodstream via a narrowed vessel with overlapped stenosis.

This work investigates the influences of polymeric heat and mass exchange on the bloodstream through a stenotic tube, using a multi-stenosed arterial model to simulate the diseased artery. To represent blood flow behavior, the constitutive equation of Williamson fluid is employed. By considering the influence of viscous dissipation on mass and heat exchange in a multi-stenosed vessel, the study aims to reveal mass transport between arterial walls and the main bloodstream. Furthermore, the interdependence of mass transport and temperature fluctuations are explained through the coupling of energy and concentration equations. The fundamental equations that define blood flow, heat transport, and mass distribution related to the velocity field are used to characterize the current biomechanical issue, along with the relevant initial and boundary data. These equations are efficiently arranged using scaling analysis and radial coordinate transformation before being numerically solved using a finite difference approach and boundary conditions. Finally, the work concludes with a thorough quantitative analysis, including graphical representations of the data and extensive discussion to assess the implications of the presented mathematical approach.

2. Geometry of stenosed vessel

The tapered arterial section with multiple stenoses in its lumen is designed as a solid tube of length L with a circular cross-section. Suppose (r, θ, z) denotes the coordinates of the material point in the polar coordinates system, with the $z-$axis aligned with the arterial axis, while θ and r reflect the circumferential and radial direction respectively. Moreover, we consider that $r = 0$ reflects the channel's axis of symmetry. The heat and mass exchange phenomena are considered by assigning temperature T_w and negligible mass concentration to the walls. In the middle of the channel, we take into account the symmetry conditions for both temperature and mass concentration. The geometry of the multiple stenoses is shown in Figure 1, with the blow mathematical expression:

$$R(z) = \begin{cases} a\left[1 - \eta_1\left\{s_i^{n-1}(z-d_i) - (z-d_i)^n\right\}\right], & d_i \le z \le d_i + s_i \\ a, & \text{otherwise} \end{cases} \tag{2.1}$$

In Eq. (2.1), a denotes the radius of the tube in the non-stenotic section, n (≥ 2) influencing the shape of the constricted profile and is known as the shape parameter (with $n = 2$ resulting in symmetric stenosis), s_i and d_i ($i = 1, 2, 3$) signify the length and site of the stenosis, respectively. The parameter η_1 is defined as.

$$\eta_1 = \frac{\delta_i\left(n^{n/n-1}\right)}{a s_i^n (n-1)}, \tag{2.2}$$

where δ_i demonstrates the maximum depth of the stenosis present at $z = a + s_i/n^{\frac{1}{n-1}}$.

3. Haemodynamic' mathematical model

The flow of incompressible fluid via a multi-stenosed section is assumed to be time-dependent, axisymmetric, and two-dimensional. As a result, the pressure, velocity, concentration, and temperature fields are defined as follows:

$$p = p(r, z, t), \mathbf{V} = (u(r, z, t), 0, w(r, z, t)), C = C(r, z, t), T = T(r, z, t), \tag{3.1}$$

where w and u are the velocity components in the axial and radial directions, respectively. By incorporating the variables mentioned above, the mass, momentum, energy, and species conservation equations can be expressed

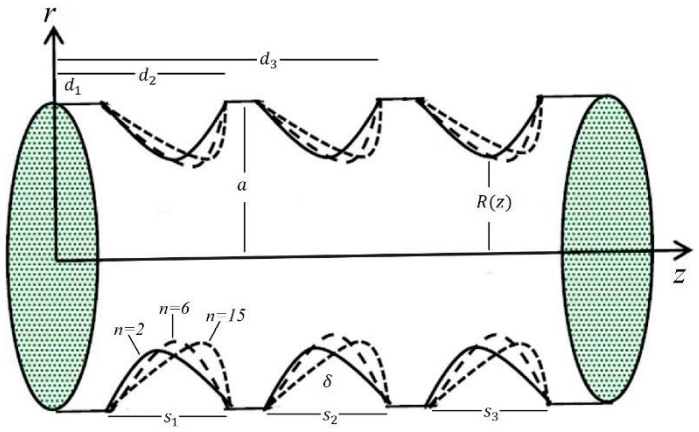

FIGURE 1. The geometry of a multi-stenosed vessel.

as [45]:

$$\frac{\partial u}{\partial r}+\frac{\partial w}{\partial z}+\frac{u}{r}=0, \tag{3.2}$$

$$\rho\left(\frac{\partial u}{\partial t}+u\frac{\partial u}{\partial r}+w\frac{\partial u}{\partial z}\right)=-\frac{\partial p}{\partial r}+\frac{1}{r}\frac{\partial}{\partial r}\ (rS_{rr})+\frac{\partial}{\partial z}\left(S_{rz}\right), \tag{3.3}$$

$$\rho\left(\frac{\partial w}{\partial t}+u\frac{\partial w}{\partial r}+w\frac{\partial w}{\partial z}\right)=-\frac{\partial p}{\partial z}+\frac{1}{r}\frac{\partial}{\partial r}\ (rS_{rz})+\frac{\partial}{\partial z}\left(S_{zz}\right)+\rho g(t), \tag{3.4}$$

$$\rho c_p\left(\frac{\partial T}{\partial t}+u\frac{\partial T}{\partial r}+w\frac{\partial T}{\partial z}\right)=S_{rr}\frac{\partial u}{\partial r}+S_{rz}\left(\frac{\partial w}{\partial r}+\frac{\partial u}{\partial z}\right)+S_{zz}\frac{\partial w}{\partial z}+K\left(\frac{1}{r}\frac{\partial T}{\partial r}+\frac{\partial^2 T}{\partial r^2}+\frac{\partial^2 T}{\partial z^2}\right), \tag{3.5}$$

$$\rho\left(\frac{\partial T}{\partial t}+u\frac{\partial T}{\partial r}+w\frac{\partial T}{\partial z}\right)=D\left(\frac{1}{r}\frac{\partial C}{\partial r}+\frac{\partial^2 C}{\partial r^2}+\frac{\partial^2 C}{\partial z^2}\right)+S_{zz}\frac{\partial w}{\partial z}+\frac{K_T D}{T_m}\left(\frac{1}{r}\frac{\partial T}{\partial r}+\frac{\partial^2 T}{\partial r^2}+\frac{\partial^2 T}{\partial z^2}\right), \tag{3.6}$$

where K, c_p, and ρ are the thermal conductivity, specific heat, and fluid density, respectively. D, K_T, and T_m are the mass (species) diffusion coefficient, thermal diffusion ratio, and mean fluid temperature, respectively. The rheology of streaming blood is assumed to obey the fundamental equation of the Williamson fluid model, which is stated as:

$$\mathbf{S}=\left[\mu_\infty+(\mu_0-\mu_\infty)\left\{1+\Gamma\left|\dot{\gamma}\right|\right\}^{-1}\right]\boldsymbol{\gamma}. \tag{3.7}$$

$$\text{where } \dot{\boldsymbol{\gamma}}=\nabla.\mathbf{V}+(\nabla.\mathbf{V})^T=\left\{\left\{2\frac{\partial u}{\partial r},\ 0,\ \ \frac{\partial u}{\partial z}+\frac{\partial w}{\partial r}\right\},\left\{0,\ 2\frac{u}{r},\ \ 0\right\},\left\{\frac{\partial u}{\partial z}+\frac{\partial w}{\partial r},\ \ 0,\ \ 2\frac{\partial w}{\partial z}\right\}\right\}, \tag{3.8}$$

$$\text{and}\dot{\gamma}=\sqrt{\frac{1}{2}trace(\dot{\boldsymbol{\gamma}}^{\mathbf{2}})}=\sqrt{2\left(\frac{\partial u}{\partial r}\right)^2+2\left(\frac{u}{r}\right)^2+2\left(\frac{\partial w}{\partial z}\right)^2+\left(\frac{\partial u}{\partial z}+\frac{\partial w}{\partial r}\right)^2}, \tag{3.9}$$

The term $g(t)$ in Eq. (3.4) signifies the body's acceleration acting along an axial direction and can be expressed as::

$$g\left(t\right)=a_g\cos(\omega_g t), \tag{3.10}$$

in which a_g is the amplitude, ϕ, and $\omega_g(=2\pi f_g)$ are the parameters for the phase angle and angular frequency of the flow respectively. The pressure gradient that appears in Eq. (3.4) can be expressed as

$$-\frac{\partial p}{\partial z} = a_1 + \mathrm{a}_2\cos(\omega_p t), \tag{3.11}$$

where a_1 specifies the constant amplitude, a_2 denotes the amplitude of the pulsatile part to account for diastolic and systolic pressure, and $\omega_p = 2\pi f_p$.

4. Boundary and initial data

The axial velocity and mass concentration are expected to be zero at the vessel wall, while the wall temperature is supposed to be constant. Furthermore, the gradients of axial velocity, temperature, and mass concentration vanish along the vessel's axis. These facts can be presented mathematically as follows:

$$\begin{aligned} &w(r,z,t) = 0, C(r,z,t) = 0, T(r,z,t) = T_w, atr = R(z), \\ &\frac{\partial w(r,z,t)}{\partial r} = 0, \frac{\partial C(r,z,t)}{\partial r} = 0, \frac{\partial T(r,z,t)}{\partial r} = 0, atr = 0. \end{aligned} \tag{4.1}$$

It is also considered that while the system is at rest, no fluid motion, heat, or mass exchange occurs. It suggests that:

$$w(r,z,t) = 0, C(r,z,t) = 0, T(r,z,t) = T_w, \text{at } t = 0. \tag{4.2}$$

5. Normalization of the problem

In order to solve the above governing equations, it is necessary to incorporate dimensionless variables, which are defined as:

$$\begin{aligned} &\overline{R} = \frac{R}{a}, \overline{r} = \frac{r}{a}, \overline{z} = \frac{z}{l_i}, \overline{t} = \frac{\omega_p t}{2\pi}, \overline{w} = \frac{w}{U_0}, \overline{u} = \frac{l_i u}{\delta_i U_0}, \overline{p} = \frac{a^2 p}{\mu_0 l_i U_0}, m = \frac{\mu_\infty}{\mu_0}, \overline{g}\left(\overline{t}\right) = \frac{\rho a^2 g(t)}{\mu_0 U_0}, \\ &\overline{S}_{\overline{rz}} = \frac{aS_{rz}}{U_0\mu_0}, \overline{S}_{\overline{rr}} = \frac{l_i S_{rr}}{U_0\mu_0}, \overline{S}_{\overline{zz}} = \frac{l_i S_{zz}}{U_0\mu_0}, \overline{S}_{\overline{\theta\theta}} = \frac{l_i S_{\theta\theta}}{\mu_0 U_0}, \overline{\dot{\gamma}} = \frac{a\dot{\gamma}}{U_0}, \overline{\delta} = \frac{\delta_i}{a}, \overline{T} = \frac{T}{T_w}, \overline{C} = \frac{C - C_1}{C_1}, \\ &e = \frac{a_1}{a_2}, \alpha = \frac{\rho a^2 \omega_p}{2\pi\mu_0}, B_1 = \frac{a_1 a^2}{\mu_0 U_0}, We = \frac{\Gamma U_0}{a}, B_2 = \frac{\rho a_g a^2}{U_0\mu_0}, B_r = \frac{\mu_0 U_0^2}{K T_w}, Pr = \frac{\mu_0 c_p}{K}, \\ &Sc = \frac{\mu_0}{\rho D}, Sr = \frac{\rho D K_T T_w}{\mu_0 T_m C_1}, \omega = \frac{\omega_g}{\omega_p}, \epsilon = \frac{a}{l_i}. \end{aligned} \tag{5.1}$$

By using the above variables, the assumption of moderate stenoses $\left(\overline{\delta} = \delta_i/a \ll 1\right)$, and the additional criterion $(\epsilon = 1)$, we get

$$\frac{\partial w}{\partial z} = 0, \tag{5.2}$$

$$\frac{\partial p}{\partial r} = 0, \tag{5.3}$$

$$\alpha\frac{\partial w}{\partial t} = -\frac{\partial p}{\partial z} + \frac{1}{r}\frac{\partial}{\partial r}\left(rS_{rz}\right) + g(t), \tag{5.4}$$

$$\alpha Pr\frac{\partial T}{\partial t} = \frac{1}{r}\frac{\partial T}{\partial r} + \frac{\partial^2 T}{\partial r^2} + Br\frac{\partial w}{\partial r}S_{rz}, \tag{5.5}$$

$$\alpha\frac{\partial C}{\partial t}=\frac{1}{Sc}\left(\frac{1}{r}\frac{\partial C}{\partial r}+\frac{\partial^2 C}{\partial r^2}\right)+Sr\left(\frac{1}{r}\frac{\partial T}{\partial r}+\frac{\partial^2 T}{\partial r^2}\right), \tag{5.6}$$

$$\text{where } S_{rz}=\left[m+(1-m)\left\{1+We\left|\frac{\partial w}{\partial r}\right|\right\}^{-1}\right]\frac{\partial w}{\partial r}. \tag{5.7}$$

The dimensionless expressions of body acceleration and pressure gradient are:

$$g\left(t\right)=B_2\left\{\cos\left(2\pi t\right)\right\}, \tag{5.8}$$

$$-\frac{\partial p}{\partial z}=B_1\left\{1+ecos\left(2\pi\omega t\right)\right\}, \tag{5.9}$$

The boundary and initial data in terms of variables (5.1), take the following form.

$$\begin{gathered}w\left(r,t\right)=0,C\left(r,t\right)=0,T\left(r,t\right)=1,\text{at } r=R(z),\\ \frac{\partial w\left(r,t\right)}{\partial r}=0,\frac{\partial C\left(r,t\right)}{\partial r}=0,\frac{\partial T\left(r,t\right)}{\partial r}=0,\text{at } r=0,\\ w\left(r,t\right)=0,C\left(r,t\right)=0,T\left(r,t\right)=0,\text{at } t=0.\end{gathered} \tag{5.10}$$

The dimensionless mathematical form of the multi-stenoses section is presented by:

$$R\left(z\right)=\begin{cases}1-\eta\left\{\left(z-h_i\right)-\left(z-h_i\right)^n\right\}, & h_i\le z\le h_i+1\\ 1, & \text{otherwise,}\end{cases} \tag{5.11}$$

where $\eta=\delta_i n^{n-1}/(n-1)$, and $h_i=d_i/l_i$. The dimensionless expressions for WSS (τ_s), volume flow rate (Q), and resistive impedance can be written as [48]:

$$\tau_s=\left[\left\{m+(1-m)\left(1+We\left|\frac{\partial w}{\partial r}\right|\right)^{-1}\right\}\frac{\partial w}{\partial r}\right]_{r=R}, \tag{5.12}$$

$$Q=\int_0^R wrdr, \tag{5.13}$$

$$\lambda=\frac{L}{l_0}\frac{(-\partial p/\partial z)}{Q}, \tag{5.14}$$

The arterial wall can be made immovable by employing a radial coordinate transformation.

$$x=r/R\ . \tag{5.15}$$

Equations (5.4)–(5.6) can be rewritten as follows by applying this transformation.

$$\alpha\frac{\partial w}{\partial t}=B_1\left\{1+ecos\left(2\pi\omega t\right)\right\}+\frac{1}{R^2x}\frac{\partial}{\partial x}\left\{x\left[m+(1-m)\left\{1+We\left|\frac{1}{R}\frac{\partial w}{\partial x}\right|\right\}^{-1}\right]\frac{\partial w}{\partial x}\right\}+B_2\left\{\cos\left(2\pi t\right)\right\}, \tag{5.16}$$

$$\alpha Pr\frac{\partial T}{\partial t}=\frac{1}{R^2}\frac{1}{x}\frac{\partial T}{\partial x}+\frac{1}{R^2}\frac{\partial^2 T}{\partial x^2}+Br\left(\frac{1}{R}\frac{\partial w}{\partial x}\right)^2\left[m+(1-m)\left\{1+We\left|\frac{1}{R}\frac{\partial w}{\partial x}\right|\right\}^{-1}\right], \tag{5.17}$$

$$\alpha\frac{\partial C}{\partial t}=\frac{1}{Sc}\left(\frac{1}{R^2}\frac{1}{x}\frac{\partial C}{\partial x}+\frac{1}{R^2}\frac{\partial^2 C}{\partial x^2}\right)+Sr\left(\frac{1}{R^2}\frac{1}{x}\frac{\partial T}{\partial x}+\frac{1}{R^2}\frac{\partial^2 T}{\partial x^2}\right), \tag{5.18}$$

The boundary and initial data in terms of variable (5.15), take the following form:

$$\begin{gathered} w(x,t)=0, C(x,t)=0, T(x,t)=1, \text{at } x=1, \\ \frac{\partial w(x,t)}{\partial x}=0, \frac{\partial C(x,t)}{\partial x}=0, \frac{\partial T(x,t)}{\partial x}=0, \text{at } x=0, \\ w(x,t)=0, C(x,t)=0, T(x,t)=0, \text{at } t=0. \end{gathered} \tag{5.19}$$

The expressions for shear stress at the wall (τ_s), volume flow rate (Q), and resistive impedance (λ) in terms of variable (5.15) can be written as:

$$\tau_s=\left[\frac{1}{R}\left\{m+(1-m)\left(1+We\left|\frac{1}{R}\frac{\partial w}{\partial x}\right|\right)^{-1}\right\}\frac{\partial w}{\partial x}\right]_{x=1}, \tag{5.20}$$

$$Q=\frac{1}{R^2}\int_0^1 wx\mathrm{d}x, \tag{5.21}$$

$$\lambda=\frac{L}{l_0}\frac{B_1\left\{1+ecos\left(2\pi\omega t\right)\right\}}{1/R^2\int_0^1 wx\mathrm{d}x}, \tag{5.22}$$

6. Numerical solution

The conversion of the partial differential equation that defines a physical phenomenon into an algebraic equation is the key to many numerical approaches. This conversion can be accomplished using a variety of approaches. One of the most popular is the finite difference approach. In this technique, the derivatives in the differential equation are replaced by suitable finite differences. The solution of the algebraic equation gives the values of the dependent variable at discrete points of the independent variables. The finite difference technique for computing Eq. (5.16) relies on the forward difference approximation for the time derivative in the following way:

$$\frac{\partial w}{\partial t}=\frac{w_j^{k+1}-w_j^k}{\Delta t}, \tag{6.1}$$

while the first and second derivatives of the spatial variable x can be discretized using the central difference approximations as follows:

$$\frac{\partial w}{\partial x}=\frac{w_{j+1}^k-w_{j-1}^k}{2\Delta x}=w_x, \frac{\partial^2 w}{\partial x^2}=\frac{w_{j-1}^k-2w_j^k+w_{j+1}^k}{(\Delta x)^2}=w_{xx}, \tag{6.2}$$

Utilizing the above difference approximations for temporal and space derivatives, Eq. (5.16) can be discretized as follows:

$$\begin{aligned} w_j^{k+1}=w_j^k+\frac{\Delta t}{\alpha}\Bigg\{B_1\left(1+ecos\left(2\pi t^k\right)\right)+\frac{1}{R^2}\frac{1}{x_j}\left(m+(1-m)\left[1+We\left|\frac{1}{R}w_x\right|\right]^{-1}\right)w_x \\ +\frac{1}{R^2}\left(m+(1-m)\left[1+We\left|\frac{1}{R}w_x\right|\right]^{-1}\right)w_{xx}+\frac{1}{R^2}w_x\frac{\partial}{\partial x}\left(m+(1-m)\left[1+We\left|\frac{1}{R}w_x\right|\right]^{-1}\right)+B_2\cos\left(2\pi t^k+\phi\right)\Bigg\}, \end{aligned} \tag{6.3}$$

where w_j^k expresses the values of w at a spatial node x_j and time interval t^k. A similar discretization scheme can be applied to Eqs. (5.17) and (5.18) which can be written as

$$T_j^{k+1} = T_j^k + \frac{\Delta t}{\alpha}\frac{1}{Pr}\left\{Br\frac{1}{R^2}\left(m+(1-m)\left[1+We\left|\frac{1}{R}w_x\right|\right]^{-1}\right)(w_x)^2 + \frac{1}{R^2}\left(T_{xx}+\frac{1}{x_j}T_x\right)\right\}, \tag{6.4}$$

$$C_j^{k+1} = C_j^k + \frac{\Delta t}{\alpha}\left\{\frac{1}{Sc}\frac{1}{R^2}\left(C_{xx}+\frac{1}{x_j}C_x\right) + Sr\frac{1}{R^2}\left(T_{xx}+\frac{1}{x_j}T_x\right)\right\}, \tag{6.5}$$

In terms of finite differences, the boundary and initial data can be approximated as:

$$\begin{gathered} w_1^k = w_2^k, T_1^k = T_2^k, C_1^k = C_2^k, \text{at } x = 0, \\ w_{N+1}^k = 0, T_{N+1}^k = 1, C_{N+1}^k = 0, \text{at } x = 1, \\ w_j^1 = 0, T_j^1 = 0, C_j^k = 0, \text{at } t = 0. \end{gathered} \tag{6.6}$$

Eqs. (6.3)–(6.5) and the boundary and initial data (6.6) can now be computed to evaluate w_j^{k+1}, T_j^{k+1}, and C_j^{k+1} with appropriately determined time increment Δt, and spatial step-size Δx. In this case, the solutions can be estimated for $(N+1)$ equally discrete points x_j with radial grid size $\Delta x = 1/(N+1)$, where $j = 1, 2, 3, \ldots,\ N+1$, $x_{N+1} = 1$, and time steps $t^k = (k-1)\,\Delta t$. To achieve the accuracy of $O(1/10^7)$, we prefer the time increment $\Delta t = 1/10^5$ and spatial step size $\Delta x = 1/40$. A detailed description of the FDM algorithm is provided in Appendix A.

7. Results and discussions

The numerical results for axial velocity, distributions of temperature and concentration, flow rate, resistive impedance, and wall shear stress (WSS) are all calculated by a computer program. The following set of values is preferred for numerical simulations of important biological contributions:

$$\begin{gathered} f_p = f_b = 1.2, d_1 = 0.375, d_2 = 1.25, d_3 = 2.125, l_1 = l_2 = l_3 = 0.5, e = 0.5, \mu_0 = 1.3, \\ \mu_\infty = 0.05, B_1 = 2, \delta = 0.2, B_2 = 2, We = 0.5, n = 2, Pr = 10, Br = 2, Sc = Sr = 0.5. \end{gathered}$$

It is of particular interest to look at the velocity profiles since they give a complete picture of the flow field. Figures 2–5 demonstrate the findings of the Williamson model for the velocity profile of circulating blood at a specified axial position ($z = 1.25$) in a stenosed vessel. The importance of body acceleration and the rheology of blood in circulation through the stenotic region has been demonstrated in Figures 2 and 3. These plots indicate that the velocity of blood increases with increasing the magnitude of body acceleration and the Weissenberg number. This is because when the body undergoes acceleration, the blood in the vessels experiences shear stress due to the change in flow direction and speed. This results in a deformation of the blood cells or fibers, causing the viscosity to change. In the case of the Williamson fluid model, as the magnitude of the acceleration increases, the deformation of the cells or fibers in the blood increases. This causes the viscosity to decrease. This decrease in viscosity results in an increase in blood velocity. Also, the Weissenberg number is a dimensionless quantity that characterizes elastic deformation in fluids. An increase in the Weissenberg number makes the blood network becomes more deformable. This means that it can align with the flow easier. This results in a decrease in viscosity and an increase in blood velocity. Figures 4 and 5 provide insights into the impact of stenosis severity (δ) on blood velocity. These figures demonstrate that increasing the size of stenosis leads to a decrease in blood velocity. This is because stenosis acts as an obstacle to blood movement and prevents blood from flowing freely in the radial direction within the vessel. Furthermore, these plots indicate that the shape of stenosis (n) also plays a significant role in influencing blood velocity. When the shape of the stenosis changes from symmetrical to asymmetrical, the velocity curves shift upwards. This indicates that the shape of

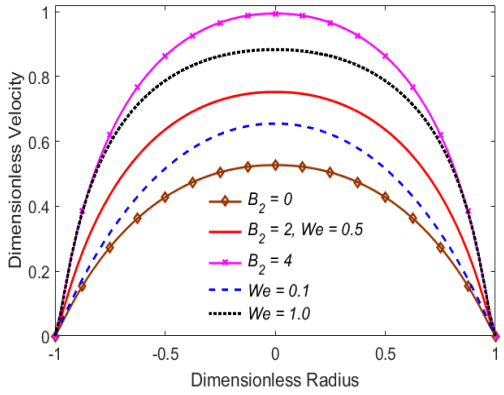

FIGURE 2. Radial velocity distribution for selected values B_2 and We.

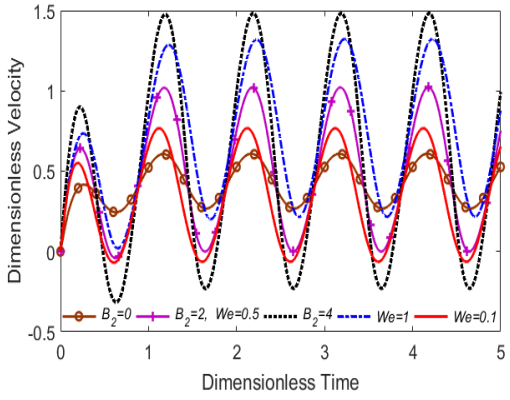

FIGURE 3. Temporal velocity profile for selected values of B_2 and We.

stenosis influences the degree of blood flow restriction, with symmetrical stenosis being more restrictive than asymmetrical stenosis.

Figures 6–9 provide graphical representations of the flow rate distribution for specific values of emergent parameters. The impacts of stenosis severity and the Wiessenberg number on volumetric flow rate are demonstrated in Figures 6 and 7. These plots reveal that an increase in the severity of stenosis (δ) leads to a significant enhancement in the volumetric flow rate, whereas elevating the Wiessenberg number (We) has the opposite effect. In other words, increasing the obstruction caused by stenosis results in a higher volume of blood flow through the affected vessel. In contrast, increasing the viscoelasticity of the fluid (represented by We) reduces the flow rate. Figures 8 and 9 illustrate that as the magnitude of body acceleration increases, there is an increase in the volume flow rate of blood through the arteries. This is because when the body is subjected to acceleration, blood flows through the arteries with greater ease because it becomes thinner and less resistant to circulation. This is due to blood's physical properties, which make it behave like a "thin" fluid when it experiences high rates of deformation. Therefore, the volume of blood flowing through the vessels increases with body acceleration. Furthermore, the figures demonstrate that at a specific axial point ($z = 1$), the volume flow rate of blood increases as the shape parameter of the stenosis is increased, *i.e.* by changing the stenosis shape from symmetrical to asymmetrical. This is because the asymmetrical shape of the stenosis causes a non-uniform distribution of fluid forces, resulting in a redistribution of the flow towards the region of lower resistance, thereby increasing the volume flow rate at that particular location.

Wall shear stress (WSS) is particularly essential in understanding the evolution of arterial diseases due to the strong connection between arteriosclerosis localization and the blood vessel wall. It refers to the drag force

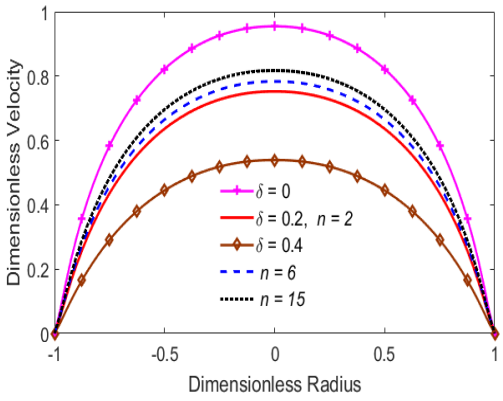

FIGURE 4. Radial distribution of velocity for selected values of δ and n.

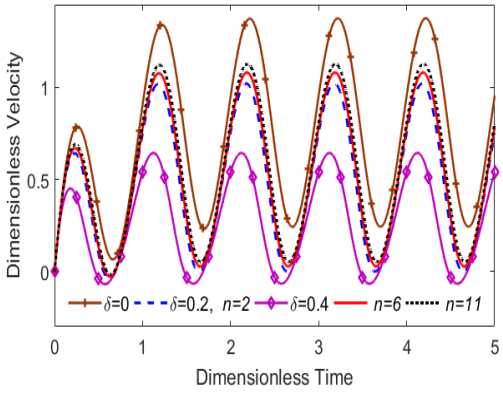

FIGURE 5. Temporal curves of velocity for selected values of δ and n.

exerted by blood flow on the inner lining of the vessel wall. Figures 10 and 11 depict the WSS distribution for three different values of δ and We. It is found that raising δ values causes the magnitude of the WSS to diminish, whereas enhancing We causes a reverse response. As the size of stenosis (δ) increases, the degree of narrowing in the vessel also deteriorates, leading to a decrease in blood flow velocity and pressure, and hence a decrease in WSS. On the other hand, as the Weissenberg number (We) increases, the fluid exhibits more non-Newtonian behavior, and its resistance to deformation also increases, leading to an increase in the magnitude of WSS. Furthermore, it has been observed that without stenosis, the magnitude of wall shear stress (WSS) remains constant throughout the vessel. However, in the presence of stenosis, the magnitude of WSS changes with the area of stenosis. It reaches its maximum at the peak of stenosis and decreases thereafter. Figures 12 and 13 demonstrate that the magnitude of wall shear stress (WSS) rises with greater values of body acceleration and shape parameters. However, this effect is more prominent in the case of body acceleration. The increase in WSS magnitude with increasing body acceleration is due to the increase in blood flow velocity and pressure caused by the acceleration of the body. Similarly, expanding the shape parameter of stenosis leads to changes in blood flow patterns and increased WSS magnitudes in certain areas, particularly at the peak of stenosis.

The resistive impedance is computed using the formula (5.22). It is a force that opposes fluid velocity. In a blood vessel, most of the resistance is caused by the diameter of the vessels. The smaller the diameter of the vessel, the heightened the resistance, which in turn decreases blood flow. The increasing size of the stenosis causes the vessel diameter in that region to decrease, thereby increasing the resistive impedance as shown in Figure 14. This graph also indicates that the intensity of resistance (λ) significantly diminishes as the amplitude

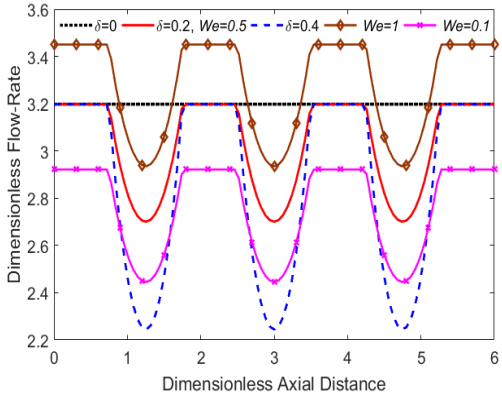

FIGURE 6. Axial distribution of flow rate for various values of δ and We.

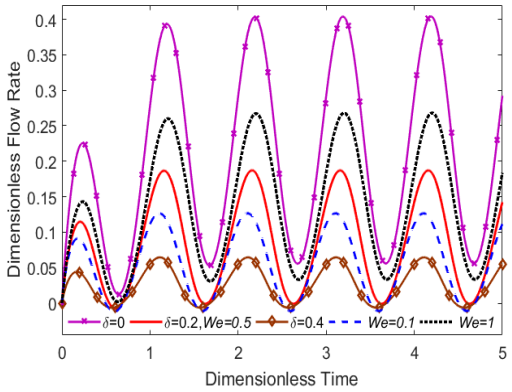

FIGURE 7. Temporal profile of low rate for specified values of δ and We.

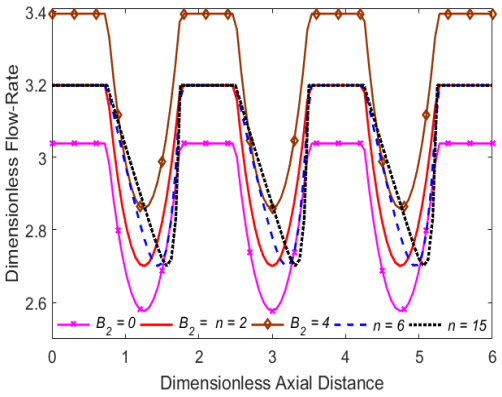

FIGURE 8. Axial profile of flow rate for various values of B_2 and n.

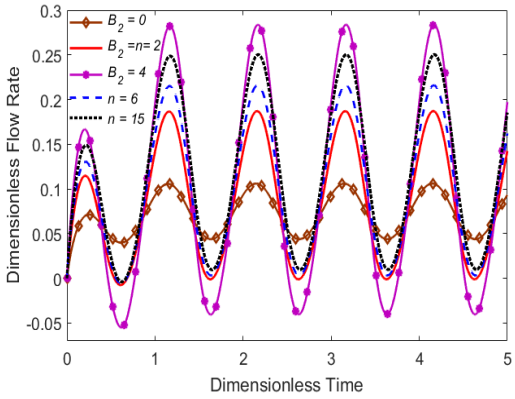

FIGURE 9. Temporal profile of flow rate for various values of B_2 and n.

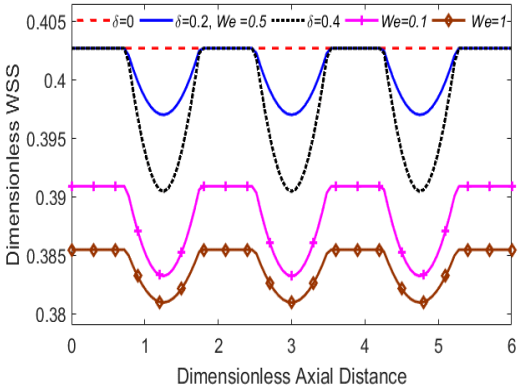

FIGURE 10. Axial profile of WSS for various values of δ and We.

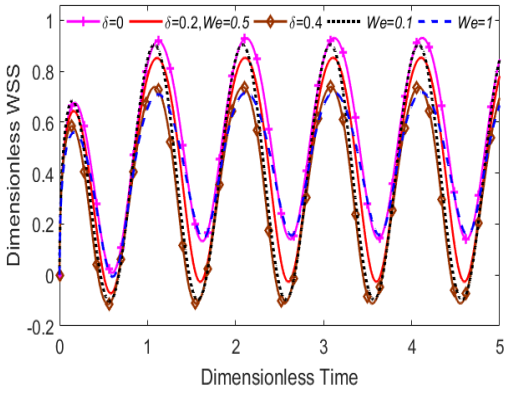

FIGURE 11. Temporal profile of WSS for various values of δ and We.

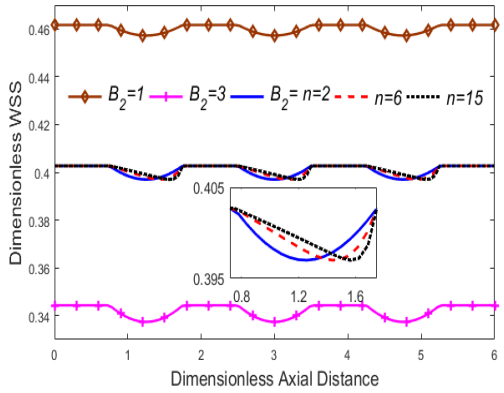

FIGURE 12. Axial profile of WSS for various values of B_2 and n

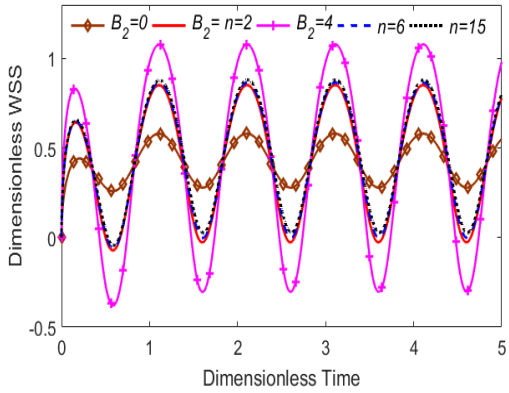

FIGURE 13. Temporal profile of WSS for various values of B_2 and n.

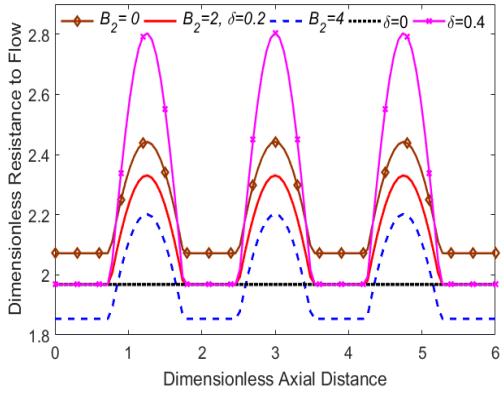

FIGURE 14. Profile of resistive impedance for various values of n and We.

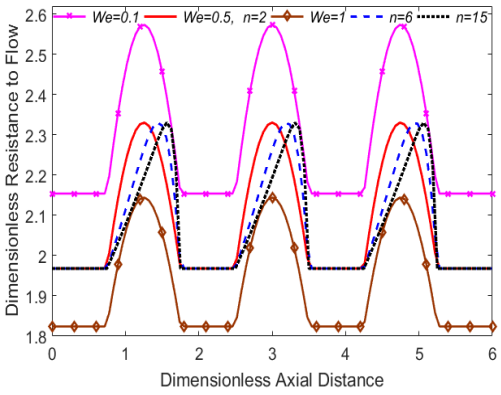

FIGURE 15. Profile of resistive impedance for various values of δ and B_2.

of acceleration enhances. Figure 15 shows the changes in resistive impedance with axial distance Z for three different values of the Weissenberg number (We) and the shape parameter (n). The graph demonstrates that the curves of resistive impedance decrease as the Weissenberg number values increase. Moreover, with symmetrical stenosis (which occurs at $n = 2$), the resistance is maximum at the center of the stenosis. However, as the shape parameter n increases, the stenosis height shifts to the downstream region. Consequently, the maximum amplitude of resistive impedance also shifts downstream.

Analyzing the distribution of heat in blood flow through stenosed arterial regions is critical for understanding the hemodynamics of blood flow, detecting the presence and severity of stenosis, and guiding treatment decisions. Therefore, the temperature profiles inside a blood vessel in relation to relevant parameters at a specific axial station ($z = 1.25$) and time ($t = 45$ sec) are illustrated in Figures 16–18. The temperature distribution through a stenotic vessel at different Pr and Br values is shown in Figure 16. The present literature on hemodynamics suggests that the Prandtl number values for blood need to be larger than 10. We then analyzed the intra-arterial blood temperature for $Pr \in [10,\ 25]$. This figure indicates that the temperature profile of blood decreases as the Prandtl number rises and increases as the Brinkman number rises. This is because the Prandtl number is a ratio of momentum diffusivity to thermal diffusivity. A higher Prandtl number indicates that the fluid is less efficient at transferring heat than momentum. Thus, increasing the Prandtl number makes heat transfer less efficient, resulting in a lower temperature profile. On the other hand, the Brinkman number measures the relative importance of viscous and thermal effects in a flow. A large Brinkman number causes viscous effects to dominate, and the flow is more adept at transferring momentum than heat. This leads to an increase in fluid temperature. Figure 17 illustrates the influences of the severity (δ) and shape (n) of stenosis on temperature distribution. This figure demonstrates that an escalation in the severity of stenosis (δ) results in a significant spike in blood temperature. This can be attributed to the fact that an increase in stenosis severity leads to an increase in obstruction of blood flow, which results in an increase in fluid resistance and a corresponding increase in heat dissipation. Therefore, more heat is generated, resulting in a higher temperature. On the other hand, the shape parameter (n) has a relatively minor effect on blood temperature because changes in this parameter mainly affect the shape of the stenosis and have a smaller impact on resistance to blood flow. Figure 18 illustrates that body acceleration has also the capacity to disturb the temperature profile. Here, it is demonstrated that enhancing the amplitude of B_2 enables the blood temperature to rise.

Mass transfer is the migration of atherogenic molecules from circulating blood to the arterial wall or vice versa. Substantial data for examining mass concentration behavior at a specific axial station $z = 1.25$ and time $t = 45$ sec are illustrated in Figures 19– 22. The impacts of the Soret number (Sr) and Schmidt number (Sc) on the concentration profile are shown in Figure 19. It is observed that the concentration profile increases as both the Soret and Schmidt numbers are increased. This is because the Soret effect is a phenomenon in which temperature gradients influence concentration distribution. A larger Soret number (Sr) corresponds to

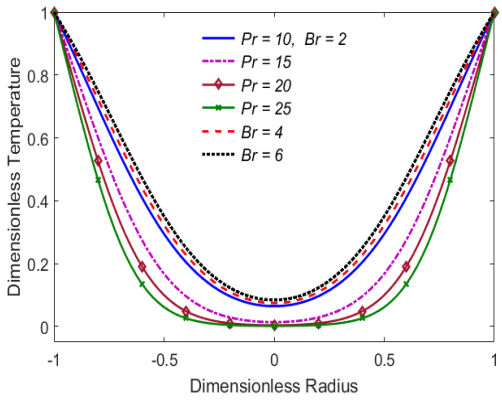

FIGURE 16. Temperature profile for specified values of Pr and Br.

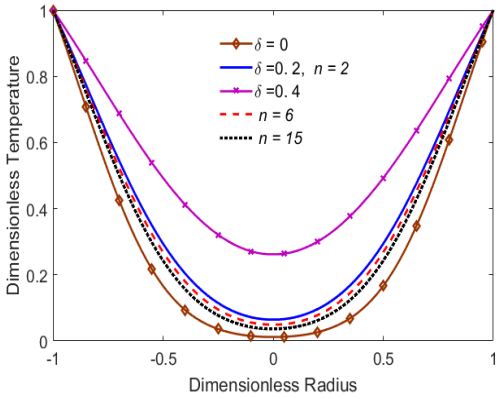

FIGURE 17. Temperature profile for specified values of δ and n.

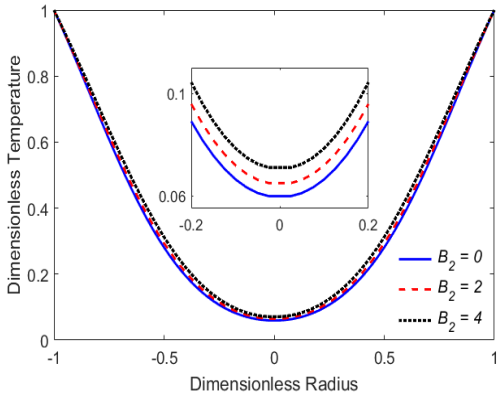

FIGURE 18. Profile of temperature for various values of B_2.

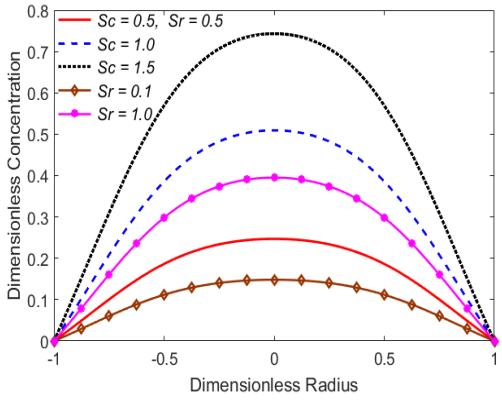

FIGURE 19. Mass concentration for various values of Sr and Sc

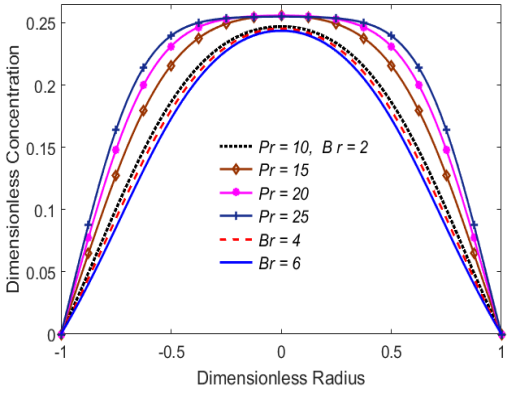

FIGURE 20. Concentration of mass for selected values of Pr and B_r.

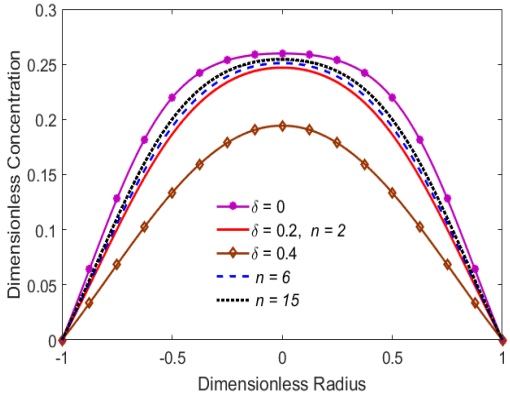

FIGURE 21. Concentration of mass for selected values of δ and n.

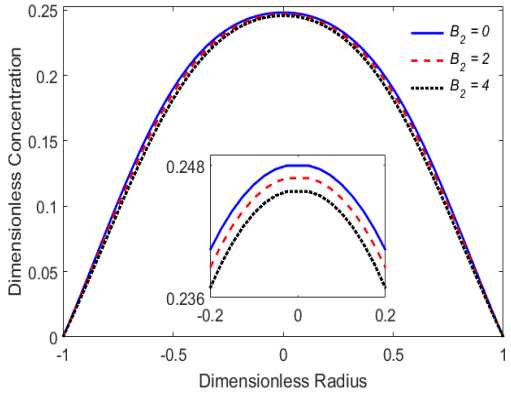

FIGURE 22. Concentration of mass for specified values of B_2.

a more intense temperature gradient, resulting in more convective movement. This widens the concentration distribution. On the other hand, the Schmidt number (Sc) relates to the diffusivity of species in a fluid. A higher Schmidt number indicates a greater diffusivity of species in a fluid. This results in a faster species transport rate and hence, a higher concentration of species. Figure 20 displays the concentration profile of the arterial segment at the neck of stenosis ($z = 1$) for different values of Prandtl and Brinkman numbers. These findings indicate that an escalation in the Brinkman number leads to a decline in mass concentration across the entire cross-section of the arterial segment. In contrast, an elevation in the Prandtl number leads to an augmentation in the solute concentration across the whole cross-section, with the exception of the central region where the curves overlap for higher Prandtl numbers ($\geq$15). The radial concentration profile for various values of severity (δ) and shape (n) of stenosis is depicted in Figure 21. It is observed that the curves of mass concentration experience a considerable decline as the values of δ increase. On the other hand, an increase in the shape parameter (n) results in an upsurge of mass concentration throughout the vessel cross-section. Figure 22 demonstrates how body acceleration affects the concentration profile. It is observed that increasing the amplitude of body acceleration results in a slight decrease in the concentration profile.

8. CONCLUSIONS

A mathematical framework for analyzing heat and mass transport phenomena in an unsteady bloodstream through a vessel having multiple stenoses has been developed. The Williamson fluid constitutive equation has been utilized to model blood rheology. The obtained initial-boundary values problem has been simulated via a numerical approach known as FDM. Flow variables such as velocity, temperature, concentration, *etc.* are quantified for emerging geometrical and rheological parameters. Based on the findings of this study, we can summarize:

– The severity of stenosis causes a decrease in blood velocity. In contrast, with high values of the shape parameter, Weissenberg number, and body acceleration, the opposite tendency is observed.

– The dimensionless flow rate distribution is directly proportional to the amplitude of body acceleration, shape parameter, and Weissenberg number. While its magnitude is inversely proportional to the size of stenosis.

– It is recognized that the intensity of the WSS is enhanced by improving the amplitude of shape parameter, body acceleration, and Weissenberg number. However, the behavior of WSS is the opposite by amplifying the severity of stenosis.

– The resistive impedance is increased by enhancing the severity of stenoses, whereas it is a diminishing function of body acceleration, shape parameter, and Weissenberg number.

– The temperature at a stenotic neck inside the vessel cross-section rises with a higher amplitude of body acceleration and severity of stenosis. Where an opposite trend is found for large values of the shape parameter.

– The temperature inside the stenotic region rises as the Brinkman number claims up. It does, however, decrease with higher Prandtl numbers.

– It is noticed that elevating the Soret and Prandtl numbers resulted in an increase in the mass distribution through vessel cross-section related to the neck of stenosis. However, it exhibits an opposite tendency by varying either the Schmidt or the Brinkman number. However, the reverse tendency is detected at larger values of the shape parameter.

Appendix A

Algorithm to solve the set of equations (6.3)–(6.5).

In order to solve the given blood flow equations numerically using the finite difference method in MATLAB, we can follow the following algorithm:

Step 1: Define the parameters and grid points

– Define the constants α, $B1$, $B2$, m, n, We, Pr, Br, Sr, and Sc.

– Define the grid points for x and t. For example, we can use $x = linspace(0,\ 1,\ Nx+1)$ and $t = linspace(0,\ T,\ Nt+1)$, where Nx and Nt are the numbers of grid points in x and t directions respectively, and T is the final time.

Step 2: Define the initial and boundary conditions

– Define the initial condition $w(x,0) = 0$ for all x.

– Define the boundary conditions $w(0,t) = w(1,t) = 0$ for all t, and $\frac{\partial w}{\partial x}(0,t) = 0$ for all t.

Step 3: Calculate the time step size and spatial step size

– Calculate the time step size $\Delta t = T/Nt$.

– Calculate the spatial step size $\Delta x = 1/Nx$.

Step 4: Set up the finite difference scheme

– Use the forward difference scheme (6.1) to discretize the time derivative term.

– Use the central difference scheme (6.2) to discretize the spatial derivative terms.

Step 5: Set up the linear system of equations

– For each time step k, set up a linear system of equations for $w(j,k+1)$, where $j = 1,\ 2,\ ...,\ Nx-1$. This can be done by discretizing the given differential equation using the finite difference scheme and rearranging the terms.

– The resulting linear system can be written in the form $Au = b$, where A is a tridiagonal matrix, u is the vector of unknowns $w(j,k+1)$, and b is the right-hand side vector.

Step 6: Solve the linear system of equations

– Solve the linear system of equations $Au = b$ using any appropriate method, such as the Thomas algorithm, LU decomposition, or iterative methods.

Step 7: Update the solution at each time step

– Once the unknowns $w(j,k+1)$ are obtained, update the solution at each time step k by setting $w(j,k+1) = u(j)$ for $j = 1,\ 2,\ ...,\ Nx-1$.

Step 8: Repeat the above steps for all time steps

– Repeat steps 5 to 7 for all time steps $k = 1,\ 2,\ ...,\ Nt$.

Step 9: Output the final solution

– Once all time steps are completed, output the final solution $w(x, T)$ for all x.

This algorithm can be implemented in MATLAB using appropriate functions and programming structures.

References

[1] O.A. Abegunrin and I. Lare Animasaun, Motion of Williamson fluid over an upper horizontal surface of a paraboloid of revolution due to partial slip and buoyancy: boundary layer analysis, in Defect and Diffusion Forum. Vol. 378. Trans Tech Publications Ltd (2017).

[2] C.H. Amanulla, N. Nagendra, R.A. Subba, O.A. Bég and A. Kadir, Numerical exploration of thermal radiation and Biot number effects on the flow of a non-Newtonian MHD Williamson fluid over a vertical convective surface. *Heat Transfer—Asian Res.* **47** (2018) 286–304.

[3] N. Ahamad, N. Ameer, S. Kamangar and I. Anjum Badruddin, The influence of curvature wall on the blood flow in stenosed artery: a computational study. *Bio-med. Mater. Eng.* **29** (2018) 319–332.

[4] R.D. Alsemiry, P.K. Mandal, H.M. Sayed and N. Amin, Numerical solution of blood flow and mass transport in an elastic tube with multiple stenoses. *BioMed. Res. Int.* bf 2020 (2020).

[5] N. Ali, A. Zaman, M. Sajid and J.J. Nieto, Unsteady non-Newtonian blood flow through a tapered overlapping stenosed catheterized vessel. *Math. Biosci.* **269** (2015) 94–103.

[6] T. Azuma and T. Fukushima, Flow patterns in stenotic blood vessel models. *Biorheology* **13** (1976) 337–355.

[7] L.H. Back, J.R. Radbill and D.W. Crawford, Analysis of oxygen transport from pulsatile, viscous blood flow to diseased coronary arteries of man. *J. Biomech.* **10** (1977) 763–774.

[8] S. Chakravarty and S. Sen, Dynamic response of heat and mass transfer in blood flow through stenosed bifurcated arteries. *Korea-Australia Rheol. J.* **17** (2005) 47–62.

[9] C.G. Caro, J.M. Fitz-Gerald and R.C. Schroter, Atheroma and arterial wall shear-observation, correlation and proposal of a shear dependent mass transfer mechanism for atherogenesis. *Proc. Roy. Soc. Lond. Ser. B. Biol. Sci.* **177** (1971) 109–133.

[10] J.C.F. Chow and K. Soda, Laminar flow and blood oxygenation in channels with boundary irregularities. *J. Appl. Mech.* **40** (1973) 843–850.

[11] R.L. Feldman, W.W. Nichols, C.J. Pepine and C.R. Conti, Hemodynamic effects of long and multiple coronary arterial narrowings. *Chest* **74** (1978) 280–285.

[12] R.L. Feldman, W.W. Nichols, C.J. Pepine, D.A. Conetta and C.R. Conti, The coronary hemodynamics of left main and branch coronary stenoses: the effects of reduction in stenosis diameter, stenosis length, and number of stenoses. *J. Thorac. Cardiovasc. Surg.* **77** (1979) 377–388.

[13] J.H. Forrester and D.F. Young, Flow through a converging-diverging tube and its implications in occlusive vascular disease—I: Theoretical development. *J. Biomech.* **3** (1970) 297–305.

[14] Z. Ismail, I. Abdullah, N. Mutapha and N. Amin, A power-law model of blood flow through a tapered overlapping stenosed artery. *Appl. Math. Comput.* **195** (2008) 669–680.

[15] W. Ibrahim and M. Negera, The investigation of MHD Williamson nanofluid over stretching cylinder with the effect of activation energy. *Adv. Math. Phys.* **2020** (2020).

[16] W. Iqbal, M.N. Naeem and M. Jalil, Numerical analysis of Williamson fluid flow along an exponentially stretching cylinder. *AIP Adv.* **9** (2019) 055118.

[17] P.E. Karayannacos, N. Talukder, R.M. Nerem, S. Roshan and J.S. Vasko, The role of multiple noncritical arterial stenoses in the pathogenesis of ischemia. *J. Thorac. Cardiovasc. Surg.* **73** (1977) 458–469.

[18] T. Kebede, E. Haile, G. Awgichew and T. Walelign, Heat and mass transfer in unsteady boundary layer flow of Williamson nanofluids. *J. Appl. Math.* **2020** (2020).

[19] K.A. Kumar, J.R. Reddy, V. Sugunamma and N. Sandeep, Simultaneous solutions for MHD flow of Williamson fluid over a curved sheet with nonuniform heat source/sink. *Heat Transfer Res.* **50** (2019).

[20] D. Kilpatrick, S.D. Webber and J.P. Colle, The vascular resistance of arterial stenoses in series. *Angiology* **41** (1990) 278–285.

[21] P.K. Mandal, An unsteady analysis of non-Newtonian blood flow through tapered arteries with a stenosis. *Int. J. Non-linear Mech.* **40** (2005) 151–164.

[22] D.A. MacDonald, On steady flow through modelled vascular stenoses. *J. Biomech.* **12** (1979) 13–20.

[23] J.C. Misra, A. Sinha and G.C. Shit, Mathematical modeling of blood flow in a porous vessel having double stenoses in the presence of an external magnetic field. *Int. J. Biomathe.* **4** (2011) 207–225.

[24] N. Mustapha, S. Chakravarty, P.K. Mandal and N. Amin, Unsteady response of blood flow through a couple of irregular arterial constrictions to body acceleration. *J. Mech. Med. Biol.* **8** (2008) 395–420.

[25] N. Mustapha, P.K. Mandal, I. Abdullah, N. NAmin and T. Hayat, Numerical simulation of generalized newtonian blood flow past a couple of irregular arterial stenoses. *Numer. Methods Part. Diff. Eq.* **27** (2011) 960–981.

[26] S. Nadeem, S. Ashiq and M. Ali, Williamson fluid model for the peristaltic flow of chyme in small intestine. *Math. Probl. Eng.* **2012** (2012).

[27] P. Nagarani and G. Sarojamma, Effect of body acceleration on pulsatile flow of Casson fluid through a mild stenosed artery. *Korea-Australia Rheol. J.* **20** (2008) 189–196.

[28] P. Owasit and S. Sriyab, Mathematical modeling of non-Newtonian fluid in arterial blood flow through various stenoses. *Adv. Diff. Eq.* **2021** (2021) 1–20.

[29] A. Ogulu and T.M. Abbey, Simulation of heat transfer on an oscillatory blood flow in an indented porous artery. *Int. Commun. Heat Mass Transfer* **32** (2005) 983–989.
[30] K. Perktold R. Peter and M. Resch, Pulsatile non-Newtonian blood flow simulation through a bifurcation with an aneurysm. *Biorheology* **26** (1989) 1011–1030.
[31] M.G. Rabby, S.P. Shupti and Md. Molla, Pulsatile non-newtonian laminar blood flows through arterial double stenoses. *J. Fluids* **2014** (2014).
[32] D.S. Sankar and U. Lee, Mathematical modeling of pulsatile flow of non-Newtonian fluid in stenosed arteries. *Commun. Nonlinear Sci. Numer. Simul.* **14** (2009) 2971–2981.
[33] A. Shafiq, A.B. Colak, T.N. Sindhu, Q.M. Al-Mdallal and T. Abdeljawad, Estimation of unsteady hydromagnetic Williamson fluid flow in a radiative surface through numerical and artificial neural network modeling. *Sci. Rep.* **11** (2021) 1–21.
[34] H. Shahzad, X. Wang, I. Sarris, K. Iqbal, M.B. Hafeez and M. Krawczuk, Study of Non-Newtonian biomagnetic blood flow in a stenosed bifurcated artery having elastic walls. *Sci. Rep.* **11** (2021) 1–13.
[35] K. Subbarayudu, S. Suneetha and P. Bala Anki Reddy, The assessment of time dependent flow of Williamson fluid with radiative blood flow against a wedge. *Propuls. Power Res.* **9** (2020) 87–99.
[36] N. Talukder, P.E. Karayanncos, R.M. Nerem and J.S. Vasko, An experimental study of the fluid dynamics of multiple noncritical stenoses. *J. Biomech. Eng.* **99** (1977) 74–82.
[37] K. Vajravelu, S. Sreenandh, K. Rajanikanth and C. Lee, Peristaltic transport of a Williamson fluid in asymmetric channels with permeable walls. *Nonlinear Anal. Real World Appl.* **13** (2012) 2804–2822.
[38] S.A. Victor and V.L. Shah, Heat transfer to blood flowing in a tube. *Biorheology* **12** (1975) 361–368.
[39] S.A. Victor and V.L. Shah, Steady state heat transfer to blood flowing in the entrance region of a tube. *Int. J. Heat Mass Transfer* **19** (1976) 777–783.
[40] V.K. Verma and P. Saraswat, Effect of a multiple stenosis on blood flow through a tube. *Int. J. Biomed. Biol. Eng.* **7** (2014) 753–756.
[41] R.Vo. Williamson, The flow of pseudoplastic materials. *Ind. Eng. Chem.* **21** (1929) 1108–1111.
[42] D.F. Young, Effect of a time-dependent stenosis on flow through a tube. *J. Eng. Ind.* **90** (1968) 248–254.
[43] W. Yonchearean and D. Young, Initiation of turbulence in models of arterial stenosis. *J. Biomech.* **12** (1979) 185–196.
[44] A. Zaman, N. Ali and M. Sajid, Slip effects on unsteady non-Newtonian blood flow through an inclined catheterized overlapping stenotic artery. *AIP Adv.* **6** (2016) 015118.
[45] A. Zaman, N. Ali, O.A. Bég and M. Sajid, Heat and mass transfer to blood flowing through a tapered overlapping stenosed artery. *Int. J. Heat Mass Transfer* **95** (2016) 1084–1095.